Journal of Magnetic Resonance 309 (2019) 106614

Contents lists available at ScienceDirect

Journal of Magnetic Resonance

journal homepage: www.elsevier.com/locate/jmr

Proton nutation spectroscopy. Application to the quantitation of water in a kaolinite sample

Maude Ferrari [a,*], Christian Moyne [a], Daniel Canet [b]

[a] Université de Lorraine, CNRS, LEMTA, F-54000 Nancy, France
[b] Université de Lorraine, CNRS, IJB, F-54000 Nancy, France

ARTICLE INFO

Article history:
Received 7 June 2019
Revised 30 September 2019
Accepted 1 October 2019
Available online 3 October 2019

Keywords:
Proton NMR nutation
Multi-line nutation spectrum
Water in clays
Paramagnetic relaxation

ABSTRACT

Nutation consists in monitoring the motion of nuclear magnetization under the application of a radio-frequency field. Depending on the amplitude of the rf field, the nutation frequency may be sensitive to the two longitudinal and transverse relaxation rates R_1 and R_2, hence the possibility of differentiating species having the same resonance frequency in the laboratory frame (the Larmor frequency) but differing by their relaxation rates, as it may occur for the composite proton NMR signal of water in complex systems. Thus, Fourier transform of the nutation curve should provide separate peaks associated with the different species involved in a composite classical NMR signal. As nutation peaks may be close to zero frequency (or even at zero frequency), their full observation requires a *complex* Fourier transform. This implies a second nutation curve, de-phased by 90° with respect to the first one, achieved here by a second nutation experiment preceded by a 90° hard pulse. Eventually, more accurate parameters are obtained by a non-linear least-squares analysis of the simple nutation experiment. This methodology is applied to water in a natural clay (kaolinite) and reveals the unexpected presence of two peaks which can be characterized by the relaxation rates derived from the line-widths of the nutation signals.

1. Introduction

The first NMR nutation experiments and the underlying theory can be found in the pioneering work of Torrey [1]. Since then, nutation experiments were mainly applied to solid state NMR for determining the quadrupolar coupling constant of quadrupolar nuclei [2] and are still nowadays used for that purpose [3,4]. It was also demonstrated that nutation experiments, through their dependence on relaxation parameters (R_1, the longitudinal relaxation rate and R_2, the transverse relaxation rate), were able to discriminate the different types of water in clays [5–7]. Furthermore, it was shown recently that pseudo-echo nutation experiments are able to provide accurately the value very short transverse relaxation times [8] when classical methods turned out to be inadequate or even fail.

A nutation experiment consists in observing the motion of nuclear magnetization in the presence of a radio-frequency (rf) field B_1 applied continuously. Viewed from the so-called rotating frame (the frame rotating around the direction of the static magnetic field B_0, at the frequency of the field B_1), this motion is similar to precession as it is merely a rotation around the B_1 field which is stationary in the rotating frame. Still viewed from the rotating frame, this B_1 field is the only magnetic field, as far as on-resonance conditions are fulfilled. Thus, the NMR signal, as a function of the duration of application of the B_1 field, oscillates at a frequency equal to $2\pi\gamma B_1$ (γ being the gyromagnetic ratio and, in this latter expression, B_1being the amplitude of the rf field). However, it turns out that, depending on B_1, the nutation curve may also depend on the longitudinal and transverse relaxation rates R_1 and R_2. In fact, the nutation frequency may become smaller than $2\pi\gamma B_1$, depending on $R_D = (R_2 - R_1)/2$ while the damping factor remains equal to $R_S = (R_1 + R_2)/2$. Thus, if the classical NMR signal is composite (involving several resonances which differ by their relaxation rates, as this is often the case for the water signal in complex systems like clays), the nutation curve is a sort of fid (free induction decay) constituted of several damped cosine functions. This should be amenable to Fourier transform. The problem is that it is a *real* Fourier transform which, by essence, leads to peaks only at positive frequencies. Although frequencies of nutation peaks are indeed positive (they may even be zero in some cases, as shown in the theoretical section), their linewidths are such that the corresponding line-shapes generally extend largely toward the negative part of the frequency domain. For properly visualizing the nutation peaks, one remedy is to resort to a *complex* Fourier transform. This requires however two different fids, one involving a cosine

* Corresponding author.
E-mail address: Maude.Ferrari@univ-lorraine.fr (M. Ferrari).

https://doi.org/10.1016/j.jmr.2019.106614
1090-7807/

modulation (the normal nutation experiment), the other with a sine modulation (obtained in this work by a hard 90° pulse preceding the normal nutation experiment). Another possibility is to model the nutation curve (of the simple experiment) with one or several damped cosine functions and to search their characteristics by non-linear least squares. These different strategies will be detailed in the first section of this paper. The second section will be devoted to a complete theoretical treatment of what can be called nutation spectroscopy with emphasis on its specificities regarding relaxation parameters as well as the possibility of quantifying the different contributions involved in the nutation curves. A special attention will be paid to nutation signals at zero frequency which may be observed when R_2 becomes very large and much larger than R_1. It will be especially shown that, in that case, the damping factor is no longer equal to R_S.

As a matter of fact, the present work is part of a project concerning the characterization of water in clays. This is a wide subject [9,10] related to many systems involving different types of water which cannot be differentiated by their chemical shifts, *i.e.* giving rise to a single NMR signal (more or less broadened). In this paper, a study by nutation spectroscopy will be applied to a natural clay (kaolinite). Kaolinite is a layered silicate mineral, with each layer made of an alternation of tetrahedral sheet of silica and of octahedral sheet of alumina forming particles of some thirty layers. After hydration, the water present in the kaolinite is not localized between the layers but only between the particles. In this system, only one type of water is expected while nutation spectroscopy reveals two different populations of water.

2. Displaying the whole nutation spectrum in the negative and positive frequency domain

As explained above, a complex Fourier transform requires the combination of two experiments with a 90° phase difference. These experiments are schematized in Fig. 1. Experiment A is the normal nutation experiment while experiment B involves an initial $\pi/2$ hard pulse which ensures the 90° dephasing of the nutation curve.

The following notations, with the quantities already defined, will be used

$$\omega_1 = \gamma B_1 \tag{1}$$

$$\omega_1^{eff} = \sqrt{\omega_1^2 - R_D^2} \tag{2}$$

Provided that ω_1 is larger than R_D, ω_1^{eff} is the frequency (in rad s^{-1}) of a given nutation signal characterized by the relaxation parameter R_D (see reference [8] and the theoretical section below). This effective frequency is the basis of nutation spectroscopy since different R_D's will lead to different peaks in the Fourier transform of the nutation curve. Note that the case $\omega_1 < R_D$ leads to a signal at zero frequency considered in detail in the next section. Anticipating the theoretical developments of this section and recognizing that it is the longitudinal component of the nuclear magnetization which is actually measured (longitudinal magnetization has been selected for sensitivity reasons), one has for the experiment A of Fig. 1:

$$m_z^A(\tau) = a_A \cos(\omega_1^{eff}\tau + \varphi_A)e^{-R_S\tau} + m_z^{st} \tag{3}$$

It will be shown that the amplitude a_A is proportional to the equilibrium magnetization m_0, that the phase φ_A is generally weak (smaller than $\pi/6$) and that the dc component m_z^{st} is also very weak. Nevertheless, both quantities can be easily corrected in the Fourier transform spectrum. A typical nutation curve (pseudo fid) is shown Fig. 2-left. It can be noted that if ω_1 would be precisely known (that is if B_1 would be accurately calibrated), R_D could be directly derived from the experimentally determined value of ω_1^{eff} (see Eq. (2)). However, the calibration of B_1 is based precisely on a nutation experiment which evidently depends on R_D. Therefore, such a calibration makes sense only if R_D is small with respect to ω_1, otherwise the value of B_1 derived of such a procedure is only approximate.

Frequencies of nutation spectra are, by nature, close to zero. Thus, the real Fourier transform of a simple nutation curve yields peaks close to zero, hardly legible and generally truncated on the left (see Fig. 2-center) because a real Fourier transform provides exclusively one side of the frequency domain (either the positive side, or the negative side which is its mirror image). Fortunately, experiment B provides a sine modulation while experiment A provides a cosine modulation. The nutation curve corresponding to experiment B has for expression (see the theoretical section below):

$$m_z^B(\tau) = a_B \sin(\omega_1^{eff}\tau + \varphi_B)e^{-R_S\tau} + m_z^{st} \tag{4}$$

a_A and a_B may be different but this can be tentatively corrected so that $m_z^A(\tau)$ and $m_z^B(\tau)$ share approximately the same amplitude a. If the dc component is (also approximately) removed from the two A and B nutation curves and if $\varphi_A \cong \varphi_B = \varphi$ (this is not always the case, see below), we can combine experiments A and B for obtaining the following complex function.

$$f(\tau) = m_z^A(\tau) + im_z^B(\tau) = ae^{i\omega_1^{eff}\tau}e^{i\varphi}e^{-R_S\tau} \tag{5}$$

The complex Fourier transform of $f(\tau)$ yields a peak at frequency (in Hz) $\nu = +\omega_1^{eff}/2\pi$ and of linewidth at half-height equal to R_S/π. The spectrum extends between $-\nu_{max}/2$ and $+\nu_{max}/2$ with $\nu_{max} = 1/2Dw$, Dw being the sampling interval of the nutation curve (Fig. 2-right). The phase φ can be corrected according to the usual procedure which combines real (Re) and imaginary (Im) parts of the Fourier transform aiming at an absorption spectrum. However, this procedure was found difficult to deal with when several peaks of different phases are present. In that case, we found useful to use the alternative method of the power spec-

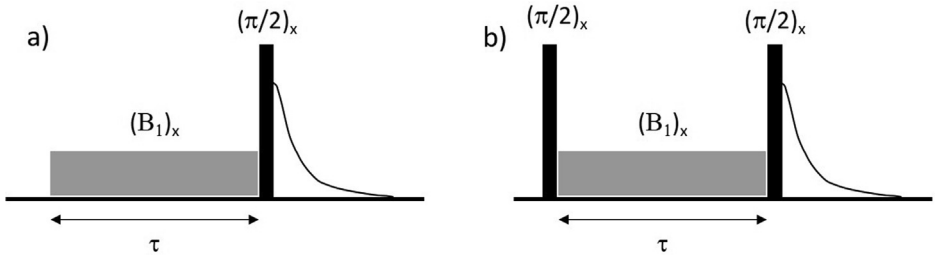

Fig. 1. (a): The simple nutation experiment: a weak rf field is applied along the x axis of the rotating frame for inducing nutation of the nuclear magnetization, assumed to be at thermal equilibrium (along the z axis) at the onset. The hard $(\pi/2)_x$ pulse allows one to select the longitudinal magnetization. (b): The normal nutation experiment with an initial $(\pi/2)_x$ pulse for obtaining a 90° dephasing of the nutation curve.

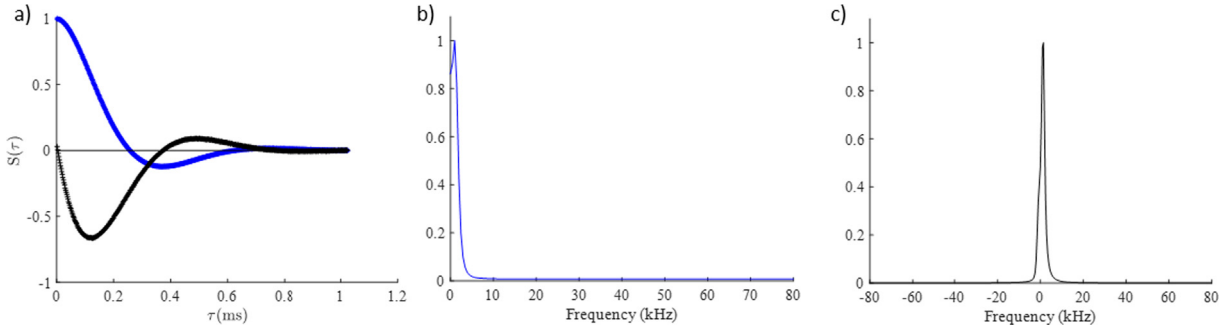

Fig. 2. (a) A typical nutation curve (pseudo fids: blue: experiment A; black; experiment B) of a water sample doped with a paramagnetic species ($MnCl_2$, 60 mM) for a B_1 field leading to low frequency oscillations. (b) The real Fourier transform of experiment A. (c) The complex Fourier transform spectrum obtained through the combination of experiments A and B. (For interpretation of the references to colour in this figure legend, the reader is referred to the web version of this article.)

trum equal to $(Re)^2+(Im)^2$. It can be shown that the power spectrum does not exhibit any dephasing but has the same lineshape and linewidth as the absorption spectrum [11]. Evidently, quantitation is lost because the height is the square of the absorption spectrum height. More precisely, $\frac{a}{R_2}$ being the height of the signal (of amplitude a) in the absorption spectrum, one has $\left(\frac{a}{R_2}\right)^2$ for the power spectrum. As will be observed in the examples given below for spectra involving two lines, the relative heights of the two peaks may be deceptive because a smaller a may be compensated by a smaller R_2, or *vice versa*. Nevertheless, quantitation will be retrieved by a least-squares analysis of experiment A (see below), the aim of this complex Fourier transform being the visualization of the nutation spectrum in terms of number of lines, of their frequency and of their line-width. Now, if $\varphi_A$and φ_B are significantly different, some complications occur. Eq. (5) must now be rewritten as

$$f(\tau) = m_z^A(\tau) + im_z^B(\tau) = ae^{-R_S\tau}\left[e^{i\omega_1^{eff}\tau}\frac{e^{i\varphi_A}+e^{i\varphi_B}}{2} + e^{-i\omega_1^{eff}\tau}\frac{e^{i\varphi_A}-e^{i\varphi_B}}{2}\right] \tag{6}$$

The power spectrum is unchanged as far as positive frequencies are concerned. However, it appears spurious image signals at negative frequencies whose intensity increases with the difference of the two phases $\varphi_A$and φ_B.

Now, it must be recognized that the useful information is indeed contained in experiment A (and Eq. (3) corrected for m_z^{st}). Therefore, for extracting the information relevant to n_{lines} lines in the nutation spectrum (constituted of n_{points} data points y_j at time $\tau_j = jDw$). The calculated pseudo fid can be expressed as

$$Y_j = \sum_{i=1}^{n_{lines}} a_{Ai}\cos(\omega_{1i}^{eff}\tau_j + \varphi_{Ai})e^{-R_{Si}\tau_j} \tag{7}$$

The various parameters can be deduced from a standard nonlinear least-squares (NLLS) procedure and used thereafter for reconstructing an absorption spectrum from $-\nu_{max}/2$ to $+\nu_{max}/2$ as a superposition of Lorentzian functions:

$$S(\nu) = \sum_{i=1}^{n_{lines}} \frac{a_{Ai}/R_{Si}}{1+4\pi^2\left(\nu-\nu_{1i}^{eff}\right)^2/R_{Si}^2} \tag{8}$$

This procedure has proved very efficient as illustrated in Fig. 3. It can be noticed that a_{Ai} provides directly the area under the corresponding Lorentzian line, thus the contribution (proportion) of species *i*.

In fact, the spectra of Fig. 3 correspond to a favorable situation for which $\varphi_A \cong \varphi_B$ in such a way that the spurious image at negative frequencies is hardly visible. In that case (a single line), the power spectrum and the reconstructed spectrum appear very similar. Another spurious signal (of very weak amplitude) is observed at zero frequency. It reflects a slightly imperfect balance between A and B nutation curves.

3. A full theory of nutation spectroscopy

Nutation takes place in the rotating frame (rotating around the fixed z axis) which is a frame in which the radio-frequency (rf) field (denoted B_1) appears stationary. The nutation process consists of a rotation around the B_1 field (if on-resonance conditions are met, as assumed throughout). If we call x the axis of the rotating frame along which lies the B_1 field, nutation takes place in the zy plane. At equilibrium, that is before the application of the rf field, nuclear magnetization lies along the z axis and will be denoted by m_0. In a general way, the components of the nuclear magnetization in the rotating frame will be denoted by (m_x, m_y, m_z).

As will be seen below, when the amplitude B_1 of the rf field is sufficiently large, $\omega_1$is simply the nutation frequency. The aim of the forthcoming calculations is to show that, with appropriate B_1 values, the actual nutation frequency may be smaller because it will depend on the relaxation rates R_1 and R_2. Under on-resonance conditions (the carrier frequency being identical to the resonance frequency), the m_x component is not created by the rf field. One has thus to consider only the m_z and m_y components which obey the following differential equations (Bloch equations).

$$\frac{dm_z}{dt} = R_1(m_0 - m_z) - \omega_1 m_y \tag{9a}$$

$$\frac{dm_y}{dt} = -R_2 m_y + \omega_1 m_z \tag{9b}$$

It has been found that, for sensitivity reasons, it was advisable to probe m_z rather than m_y. Hence, the observing 90° hard pulse, after the nutation interval, in the experiments sketched in Fig. 1 and the m_z differential equation built from (9a) and (9b):

$$\frac{d^2m_z}{dt^2} + (R_1+R_2)\frac{dm_z}{dt} + \left(R_1R_2+\omega_1^2\right)\left(m_z - m_z^{st}\right) = 0 \tag{10}$$

with $m_z^{st} = \frac{R_1R_2}{\omega_1^2+R_1R_2}m_0$

The following notations regarding the sum and the difference of the relaxation rates are recalled for convenience:

$$R_{S,D} = \frac{1}{2}(R_2 \pm R_1) \tag{11}$$

From the characteristic equation of (13), two situations must be envisaged: $\omega_1 > R_D$ and $\omega_1 < R_D$.

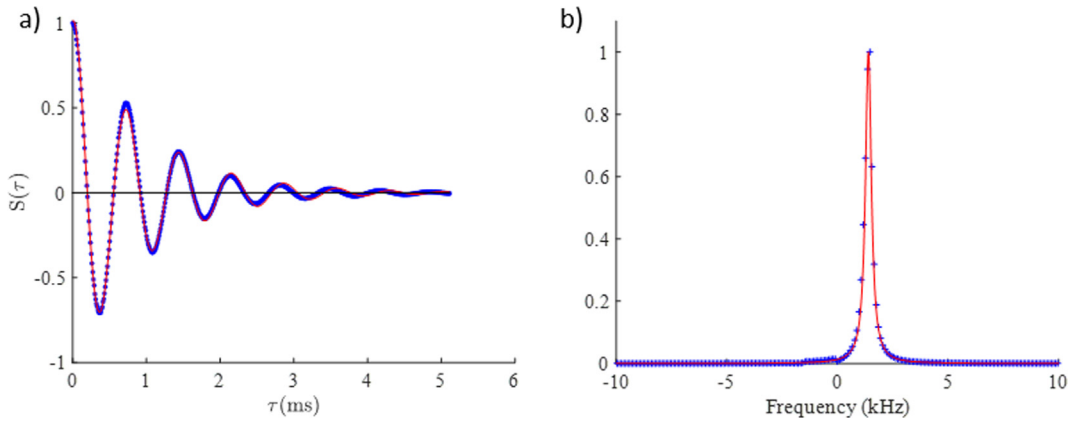

Fig. 3. (a) A typical nutation curve (experiment A) of a water sample doped with a paramagnetic species ($MnCl_2$, 10 mM) for a B_1 field leading to more pronounced oscillations than in Fig. 2. Blue: experimental data points; red; reconstructed pseudo-fit with parameters obtained through a least-squares analysis. (b) Blue dots: nutation power spectrum obtained from the complex Fourier transform of experiments A and B. Red: reconstructed nutation spectrum resulting from the least squares analysis of experiment A. For visualization purposes, both spectra have been normalized to the same maximum value. In this figure and in the following, the point size represents roughly the experimental uncertainty. (For interpretation of the references to colour in this figure legend, the reader is referred to the web version of this article.)

(1) $\boldsymbol{\omega_1 > R_D}$

The solution of (10) is oscillatory:

$$m_z(t) = m_z^{st} + e^{-R_S t}\left\{ [m_z(0) - m_z^{st}]\cos\omega_1^{eff} t + \frac{1}{\omega_1^{eff}}[R_S(m_0 - m_z^{st}) + R_D(m_z(0) - m_0) - \omega_1 m_y(0)]\sin\omega_1^{eff} t \right\} \quad (12)$$

Experiment A: $m_z(0) = m_0$, $m_y(0) = 0$

$$m_z(t) - m_z^{st} = a_A e^{-R_S t}\cos\left(\omega_1^{eff} t + \varphi_A\right)$$

$$a_A = (m_0 - m_z^{st})\sqrt{1 + \left(\frac{R_S}{\omega_1^{eff}}\right)^2} \quad (13)$$

$$\tan\varphi_A = -\frac{R_S}{\omega_1^{eff}}$$

Experiment B: $m_z(0) = 0$, $m_y(0) = m_0$

$$m_z(t) - m_z^{st} = -a_B e^{-R_S t}\sin\left(\omega_1^{eff} t + \varphi_B\right)$$

$$a_B = \sqrt{(m_z^{st})^2 + \left(\frac{1}{\omega_1^{eff}}\right)^2\left[(R_S - R_D - \omega_1)m_0 - R_S m_z^{st}\right]^2} \quad (14)$$

$$\tan\varphi_B = -\frac{m_z^{st}\omega_1^{eff}}{(R_S - R_D - \omega_1)m_0 - R_S m_z^{st}}$$

From these expressions, it can be seen that, if ω_1 is sufficiently large with respect to the relaxation rates, one has effectively: $m_z^{st} \cong 0$, $a_A \cong a_B \cong m_0$ and $\varphi_A \cong \varphi_B \cong 0$. Otherwise, one has to face the problems mentioned in the previous section. In any event, the numerical analysis of experiment A, as described in the previous section, seems to be the method of choice as far as quantitation is required (a_A remains in all instances close to m_0). On the other hand, the linewidth at half height will provide R_S:

$$lw = \frac{R_S}{\pi} \quad (15)$$

As R_D could in principle be deduced from ω_1^{eff} (see Eq. (2); this would however require an accurate calibration of the B_1 field), a precise analysis of experiment A should lead to m_0, and again in principle to R_1 and R_2.

(2) $\boldsymbol{\omega_1 < R_D}$

This condition is encountered in some instances, especially when R_2 becomes very large and much larger than R_1. The solution of (10) is no longer oscillatory and the frequency of the nutation signal is zero. One has

$$m_z(t) - m_z^{st} = e^{-R_S t}(a_z e^{-R_D^{eff} t} + b_z e^{+R_D^{eff} t}) \quad (16)$$

$$\text{with} \quad R_D^{eff} = \sqrt{R_D^2 - \omega_1^2} \quad (17)$$

a_z and b_z are determined from the initial conditions $m_z(0)$ and $\left(\frac{dm_z}{dt}\right)_{t=0}$:

$$a_z = -\frac{R_s - R_D^{eff}}{2R_D^{eff}}[m_z(0) - m_z^{st}] - \frac{R_1}{2R_D^{eff}}[m_0 - m_z(0)] + \frac{\omega_1}{2R_D^{eff}}m_y(0) \quad (18)$$

$$b_z = \left(1 + \frac{R_s - R_D^{eff}}{2R_D^{eff}}\right)[m_z(0) - m_z^{st}] + \frac{R_1}{2R_D^{eff}}[m_0 - m_z(0)] - \frac{\omega_1}{2R_D^{eff}}m_y(0) \quad (19)$$

Experiment A: $m_z(0) = m_0$, $m_y(0) = 0$

$$a_z = -\frac{R_s - R_D^{eff}}{2R_D^{eff}}[m_0 - m_z^{st}] \quad \text{and} \quad b_z = \left(1 + \frac{R_s - R_D^{eff}}{2R_D^{eff}}\right)[m_0 - m_z^{st}]$$

Assuming that R_2 is much larger than R_1 and ω_1, we can see that $\frac{R_s - R_D^{eff}}{2R_D^{eff}}$ is close to zero and use the following approximation (neglecting further m_z^{st} with respect to m_0)

$$m_z(t) - m_z^{st} \cong -m_0 e^{-(R_s - R_D^{eff})t} \quad (20)$$

Therefore, m_0 can be approximately deduced from experiment A which can be again considered as quantitative.

Moreover, still assuming that R_D is much larger than ω_1 and performing first order expansions, we obtain for the two exponents of Eq. (16): $e^{-(R_s - R_D^{eff})t} \cong e^{-(R_1 + \frac{\omega_1^2}{2R_D})t}$ and $e^{-(R_s + R_D^{eff})t} \cong e^{-(R_2 - \frac{\omega_1^2}{2R_D})t}$, this latter term decreasing very rapidly. Thus, the linewidth at half height can be approximated as

$$lw \cong \frac{1}{\pi}(R_1 + \frac{\omega_1^2}{2R_D}) \quad (21)$$

It can be seen that the linewidth should decrease when B_1 decreases. Moreover, carrying out at least two experiment with different B_1 values should lead to the two relaxation rates, provided that ω_1^2 is known with a reasonable accuracy.

Experiment B: $m_z(0) = 0$, $m_y(0) = m_0$

$$a_z = \frac{\omega_1 - R_1}{2R_D^{eff}} m_0 + \frac{R_s - R_D^{eff}}{2R_D^{eff}} m_z^{st} \text{ and}$$

$$b_z = -\frac{\omega_1 - R_1}{2R_D^{eff}} m_0 - (1 + \frac{R_s - R_D^{eff}}{2R_D^{eff}}) m_z^{st}.$$

With the same approximations as above, one has

$$a_z \cong -b_z \cong \frac{\omega_1 - R_1}{2R_D^{eff}} m_0.$$

The resulting expression is somewhat more complicated than for experiment A and not really amenable to the determination of pertinent parameters.

$$m_z(t) - m_z^{st} \cong \frac{\omega_1 - R_1}{2R_D^{eff}} m_0 e^{-R_s t}(e^{-R_D^{eff} t} - e^{+R_D^{eff} t}) \quad (22)$$

Thus, experiment B will serve (as usual) to construct, along with experiment A, a set of complex data, the Fourier transform of which being used for visualizing purposes.

4. Results

The sample of kaolinite which is investigated is supposed to involve only one type of water. It turns out that the nutation spectrum contains the expected signal with relaxation parameters usual for water in clays but also an additional signal at zero frequency characteristic of a very large transverse relaxation rate, still much larger than the longitudinal relaxation rate. This is shown in Fig. 4

The fact that the power spectrum is somewhat close to the reconstructed spectrum is here especially deceptive. As explained in the first section, this is due for the peak at zero frequency (in the power spectrum) to a smaller R_2 compensating a smaller amplitude. In any event, as shown above, reliable parameters are preferentially obtained from the least-squares analysis of experiment A. It is particularly interesting to notice that, in agreement with theory, the line at zero frequency is paradoxically sharp. As shown In the theory section, this is due to the fact that the linewidth is dominated by R_1 and not R_2 (with here $R_1 \ll R_2$). Now and as stated above, the amplitudes a_i are nothing else than the peak areas. Using the values obtained from the least-squares analysis of experiment A, we arrive at the conclusion that the peak at zero frequency represents about 30% of the total amount of water (this proportion has been calculated from $\frac{a_1}{a_1+a_2}$). This is the amazing result of this study. A single nutation peak was expected (the high frequency peak with relaxation rates around 3 ms^{-1}) corresponding to water interacting with the clay surface. In addition, a peak at zero frequency is observed implying a very large transverse relaxation rate ($R_2 > 40\ ms^{-1}$) the origin of which, as indicated by recent observations, originate from an heterogeneous distribution of paramagnetic species which are responsible for the spin relaxation phenomena affecting water in these systems. The composition of the actual kaolinite sample confirms the presence of paramagnetic species such as Fe_2O_3 or TiO_2 [12,13]. This signal tends to weaken several weeks after the sample has been hydrated (proportions go from 30:70 to 10:90) and that, at the same time, the relaxation rate corresponding to the signal at a positive frequency tends to increase. This is illustrated by the series of spectra shown in Fig. 5. The rf amplitude is not sufficient for satisfying the condition $\omega_1 > R_D$ and thus moving to higher frequency the signal at zero frequency. After several months, the signal at zero frequency has almost totally disappeared indicating that the clay sample tends to become homogeneous (see Fig. 5b).

Concerning the spectra of Fig. 5, some differences occur between the power spectrum and the recalculated spectrum (resulting from the least-squares analysis). This is in agreement with the previous considerations: contrary to the spectrum of Fig. 4, the weaker amplitude of the signal at zero frequency is no longer compensated for by its transverse relaxation rate. Data corresponding to the spectra of Figs. 4 and 5 are gathered in Table 1.

Some information concerning relaxation rates can be deduced from the data of Table 1. From Eq. (21) where ω_1 can be replaced by $2\pi\nu_2$, we can write for the peak at zero frequency

$$R_D = 2\pi \frac{\nu_{2a}^2 - \nu_{2b}^2}{lw_{1a} - lw_{1b}} \quad (23)$$

where *a* and *b* refer to two different values of the B_1 field. Using the data at $B_1 = 20\%$ and $B_1 = 50\%$, we obtain for R_D a value around 2600 ms^{-1} and then, directly from (21), a value for R_1 around 1 ms^{-1}. Owing to this latter value, R_D can be safely assimilated to $R_2/2$, thus $R_2 = 5200\ ms^{-1}$, an extraordinary large value which can only arise from paramagnetic relaxation. We turn now to the peak at positive frequencies, the linewidth of which is equal to $\frac{R_S}{\pi}$ (Eq. (15)) yielding R_2 values around 4 ms^{-1}, still assuming $R_1 \ll R_2$ (this

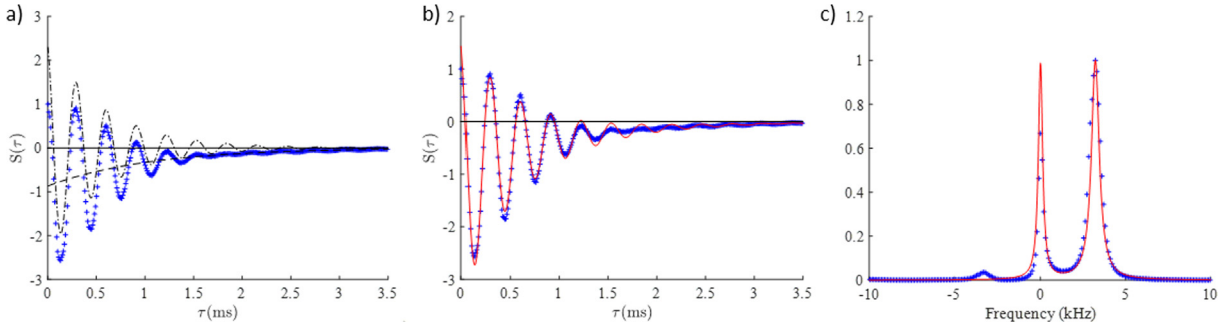

Fig. 4. (a): Kaolinite nutation curve (experiment A, data points in blue) for B_1 = 20% of the maximum available value ($\gamma B_1 \approx 3.3$ kHz) clearly showing oscillations superposed to a contribution at zero frequency. The dashed black curves correspond to the reconstructed (from a least-squares analysis) nutation curves of both contributions. (b) The experimental nutation curve (blue dots) with the total pseudo-fid (red curve) reconstructed from the least-squares analysis. (c) Corresponding nutation spectra. Blue dots: nutation power spectrum obtained from the complex Fourier transform of experiments A and B. Red: reconstructed nutation spectra resulting from the least squares analysis of experiment A. For visualization purposes, both spectra have been normalized to the same maximum value. (For interpretation of the references to colour in this figure legend, the reader is referred to the web version of this article.)

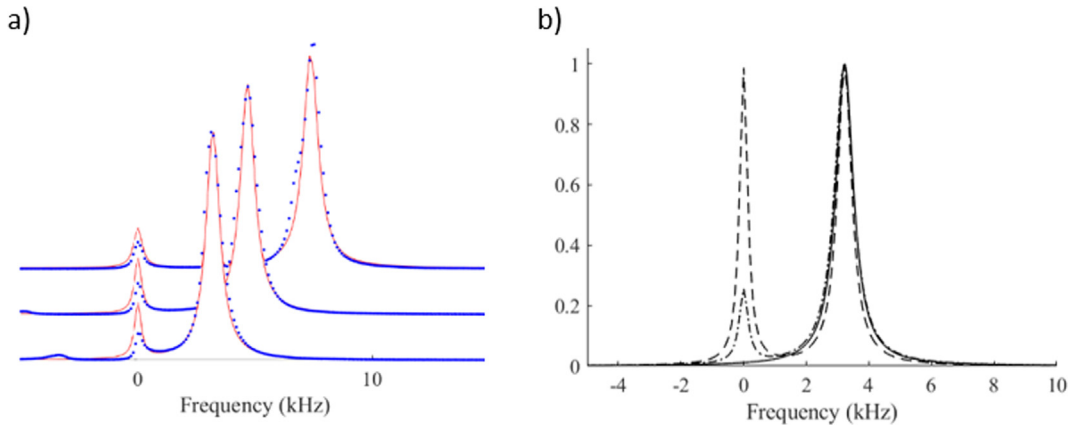

Fig. 5. (a) Spectra obtained two months after the one of Fig. 4. From bottom to top: B_1 = 20%, 30% and 50% of the maximum available value. Blue dots: nutation power spectra obtained from the complex Fourier transform of experiments A and B. Red: reconstructed nutation spectra resulting from the least squares analysis of experiment A; For visualization purposes, the power spectrum and the reconstructed spectrum have been normalized to the same maximum value. (b) Spectra showing the sample evolution after its initial hydration forB_1 = 20%: time zero (–), three months (-.-), five months (-). (For interpretation of the references to colour in this figure legend, the reader is referred to the web version of this article.)

Table 1
Peak at zero frequency: $p_1 = a_1/(a_1 + a_2)$; lw_1: linewidth at half-height. lw_2: linewidth at half-height of peak at frequency ν_2.

Experiment	p_1	lw_1 (kHz)	ν_2 (kHz)	lw_2 (kHz)
Fig. 4 B_1: 20%	0.33 ± 0.03	0.30 ± 0.01	3.22 ± 0.01	0.56 ± 0.01
Fig. 5 B_1: 20%	0.12 ± 0.05	0.33 ± 0.01	3.20 ± 0.01	0.72 ± 0.01
Fig. 5 B_1: 30%	0.11 ± 0.05	0.36 ± 0.01	4.68 ± 0.01	0.74 ± 0.01
Fig. 5 B_1: 50%	0.10 ± 0.09	0.43 ± 0.02	7.37 ± 0.02	0.77 ± 0.01

has been checked by a direct measurement of R_1 from the normal NMR spectrum in which water corresponding to this peak is exclusively visible, because the nutation peak at zero frequency is much too broad to be visible). Finally, assuming dipolar relaxation and the same relaxation mechanism for both peaks (affecting the water protons located at a distance r from the unpaired electron of the paramagnetic species) implies a dependence in $1/r^6$. The ratio of the two R_2 values (5200:4) can be used to derive an estimate of the ratio of the distances between water and the location of paramagnetic species within the clay material. We obtain r_1/r_2 around 0.3, meaning that water molecules corresponding to the peak at zero frequency are roughly three times closer to the paramagnetic species than those corresponding to the peak at positive frequencies. This is however a crude estimate which should be refined with regard to the sample heterogeneity.

5. Experimental

The NMR experiments were performed with a spectrometer equipped with a 4.7 T Oxford magnet (proton resonance frequency: 200 MHz) and an NMR cube console manufactured by RS^{2}D. The 90° pulse duration is 24 μs (corresponding to 85% of the maximum B_1 field). All experiments were carried out at 298 K. The kaolinite clay sample come from Warren County in Georgia in USA (KGa-2 kaolinite reference from the Source Clay Repository of The Clay Minerals Society). The elemental composition of this clay minerals has been described in several publications [12,13]. The sample is prepared and packaged as described in the article of Porion *et al.* [14]. The sample of kaolinite used for these first measurements was hydrated at 100%. Nutation curves were obtained with 512 data points, the sampling interval (increment of the duration of the rf field application) being 10 ms. Experiments were carried out at different B_1 values as indicated in the text.

In all these experiments, when a rf field is applied for a non-negligible time interval (contrary to hard pulses), sample temperature may be a problem. Several points can be mentioned which explain why no disturbance was observed even at large τ values (see Fig. 1): (i) the transmit coil is designed for 10 mm o.d. sample tubes whereas 5 mm o.d. sample tubes are used for the present experiments making the rf source relatively far from the sample (initially, for avoiding radiation damping effects), (ii) an air flow is systematically employed, (iii) large rf amplitudes were not used so as to prevent dielectric heating and amplifier dips. The latter could actually be avoided by using a coil of smaller diameter but at the risk of dielectric heating. Also, with the present probe, B_1 inhomogeneity is negligible for our current experiments (as shown previously [8]). Finally, B_0 inhomogeneity of course affects experiments involving *precession* but is known to have little effect on *nutation* experiments.

6. Conclusion

The aim of this study was to devise an appropriate methodology for obtaining nutation spectra, *i.e.* a series of peaks when the nutation curve arises from a single NMR signal involving several contributions which differ by their relaxation rates. We have emphasized that a simple (real) Fourier transform is not convenient because it does not provide the negative part of the frequency domain and, as a consequence, would lead to severely truncated peaks. The idea was then to use a complementary experiment affording a sine modulation while the simple nutation experiment involves a cosine modulation. This is easily accomplished by adding a hard 90° pulse at the beginning of the simple nutation experiment. Combining these two experiments permits a complex Fourier transform yielding clear spectra including the negative part of the frequency domain. This is especially valuable for a signal at zero frequency which can occur whenever R_2 is very large and much larger than R_1. However, as shown theoretically, an accurate quantitation is not attainable by this method which in addition generates small artefacts. Thus, the complex Fourier transform serves merely for visualizing purposes, that is for determining the number of contributions to the nutation curve and obtaining a first estimate of their characteristics. Thereafter, the method of choice for arriving at quantitative and reliable results is to analyse

the simple nutation experiment by least-squares and to reconstruct an appropriate spectrum. This was successfully applied to the clay sample investigated in this study (which constitutes a good test since, fortunately, it involves two signals, including a signal at zero frequency). A further advantage of such a method is its ability to separate signals which would overlap in the spectrum obtained by Fourier transform. It can be further noticed that the discrimination of neighboring signals can be improved by changing the amplitude of the rf field (see Fig. 5). Concerning spin relaxation, the method provides a very good estimate of both relaxation rates R_1 and R_2, as far as one has to deal with a signal at zero frequency. By contrast, for signals at positive frequencies, the method provides only half the sum of R_1 and R_2. If both relaxation rates are required, it can be anticipated that combining inversion-recovery or saturation-recovery with the simple nutation experiment would easily yield the R_1 value for each signal. Concerning the clay sample serving as an example in this study, these relaxation rates have allowed us to characterize the possible heterogeneity of the sample and to delineate the interactions between water and the paramagnetic species present in the clay material.

Declaration of Competing Interest

The authors declare that they have no known competing financial interests or personal relationships that could have appeared to influence the work reported in this paper.

Acknowledgement

The authors thank Thomas Dabat et Eric Ferrage (IC2MP, Poitiers, France) for the packaging of kaolinite samples.

The Carnot Institute ICEEL by project: MultiEC-HYDRO and the CNRS interdisciplinary "défi Needs" through its "MiPor" program (Project TRANSREAC) are acknowledged for providing financial support for this study.

References

[1] H.C. Torrey, Transient nutations in nuclear magnetic resonance, Phys. Rev. 76 (1949) 1059–1068.
[2] W.S. Veeman, Quadrupole nutation NMR in solids, Z. Naturforsh 47a (1992) 353–360.
[3] E.S. Blaakmeer, W. Franssen, A. Kentgens, Quadrupolar nutation NMR to discriminate central and satellite transitions: spectral assignments for a Ziegler-Natta catalyst, J. Magn. Reson. 281 (2017) 199–208.
[4] W. Franssen, Y. Rezus, A. Kentgens, High radio-frequency field strength nutation NMR of quadrupolar nuclei, J. Magn. Reson. 273 (2016) 33–39.
[5] G. Trausch, D. Canet, A. Cadène, P. Turq, Separation of a ^{1}H composite signal by nutation experiments under low amplitude radio-frequency fields. Application to water in clays, Chem. Phys. Lett. 433 (2006) 228–233.
[6] G. Trausch, D. Canet, ^{1}H nutation experiments under low-amplitude radiofrequency fields. Quantitative analysis of a complex NMR signal arising from water in clays and including a Pake doublet, Magn. Reson. Imag. 25 (2007) 525–528.
[7] M. Fleury, D. Canet, Water orientation in smectites using NMR nutation experiments, J. Phys. Chem. C 118 (2014) 4733–4740.
[8] M. Ferrari, C. Moyne, D. Canet, Measurement of short transverse relaxation times by pseudo-echo nutation experiments, J. Magn. Reason. 292 (2018) 8–15.
[9] V. Olphen, An Introduction to Clay Colloid Chemistry: For Clay Technologists, Geologists, and Soil Scientists, Wiley, New York, 1977.
[10] J.K. Mitchell, Fundamentals of Soil Behaviour, Wiley, New York, 1993.
[11] see for instance: F. Guenneau, P. Mutzenhardt, D. Grandclaude, D. Canet, Measurement of longitudinal and rotating-frame relaxation times through fully J-decoupled homonuclear spectra J. Magn. Reson. 140 (1999) 250–258.
[12] A.R. Mermut, A.F. Cano, Baseline studies of the clay minerals society source clays: chemical analyses of major elements, Clay Clay Miner. 49 (2001) 381–386.
[13] S.T. Chipera, D.L. Bish, Baseline studies of the clay minerals society source clays: powder X-ray diffraction analysis, Clay Clay Miner. 49 (2001) 398–409.
[14] P. Porion, E. Ferrage, F. Hubert, E. Tertre, T. Dabat, A.M. Faugère, F. Condé, F. Wermont, A. Delville, Water mobility within compacted clay samples: multiscale analysis exploiting ^{1}H NMR pulsed gradient spin echo and magnetic resonance imagingof water density profiles, ACS Omega 3 (2018) 7399–7406.